Hindawi
Journal of Nanomaterials
Volume 2019, Article ID 1049142, 11 pages
https://doi.org/10.1155/2019/1049142

Research Article

Eco-Friendly, Green Packaging Materials from Akaganeite and Hematite Nanoparticle-Reinforced Chitosan Nanocomposite Films

G. T. D. Chandrakumara,[1,2] D. M. S. N. Dissanayake,[1,2] M. M. M. G. P. G. Mantilaka,[1,2] R. T. De Silva,[1] H. M. T. G. A. Pitawala,[2,3] and K. M. Nalin de Silva[1,4]

[1]*Sri Lanka Institute of Nanotechnology (SLINTEC), Nanotechnology and Science Park, Mahenwatte, Pitipana, Homagama, Sri Lanka*
[2]*Postgraduate Institute of Science, University of Peradeniya, Peradeniya, Sri Lanka*
[3]*Department of Geology, Faculty of Science, University of Peradeniya, Peradeniya, Sri Lanka*
[4]*Department of Chemistry, University of Colombo, Colombo, Sri Lanka*

Correspondence should be addressed to M. M. M. G. P. G. Mantilaka; mantilaka@gmail.com

Received 8 September 2019; Revised 18 November 2019; Accepted 3 December 2019; Published 23 December 2019

Academic Editor: Francesco Marotti de Sciarra

In this study, chitosan nanocomposite thin films were successfully fabricated by incorporating hematite nanoparticles (HNPs) and akaganeite nanoparticles (ANPs) as reinforcing fillers using the solution casting method. HNPs and ANPs were synthesized via a urea-assisted synthesis route using naturally occurring ferruginous laterites. Scanning electron microscopic (SEM) images indicated the spherical to subhexagonal morphology of the HNPs and rice-like morphology of the ANPs. X-ray diffractograms indicate the crystalline structure of iron oxides as hematite and akaganeite. Tensile tests were carried out to evaluate the mechanical properties of the nanocomposite films where maximum tensile stress of the chitosan/HNP composites was improved as high as 35.7% while chitosan/ANP composites indicated 43.5%. Thermal decomposition curves obtained by thermogravimetric analysis (TGA) indicate that the thermal stability of the nanocomposites has improved remarkably compared to neat chitosan films. Furthermore, these nanocomposites exhibited excellent UV barrier properties as identified by UV-visible spectrometry. Fourier-transform infrared (FTIR) spectroscopic results are evident in the presence of Fe-O bond in the wavenumber around 480-500 cm^{-1}, and the result also indicated that the nanofillers interact with the chitosan matrix via hydrogen bonding, which enhanced the physical properties of the nanocomposites. Incorporation of iron oxide nanoparticle varieties into chitosan has led to improvements of certain physical and chemical properties, which make chitosan a promising material for packaging applications.

1. Introduction

Over several decades, various biodegradable materials have gained considerable attention as alternatives for petrochemical-based packaging materials [1]. Production of biopolymeric packaging films provides a number of economic and environmental benefits. Chitosan (CH) is one of the key naturally derived green polymers used in the synthesis of packaging materials [2–4]. It is the linear polymer of β-(1-4)-2-acetamido-2-deoxy-D-glucopyranose synthesized by deacetylation of chitin, the second most abundant polysaccharide in nature. Chitin is extracted by the exoskeleton of crustaceans such as shrimps and crab shells [5–7]. Chitosan exhibits superior properties such as nontoxicity, biodegradability, biocompatibility, antiviral, and antimicrobial properties [8–12]. This unique biopolymer is widely applied in various fields including agriculture [13], food packaging [14–16], textiles [10], bioengineering, and medicine [17, 18].

Although CH can easily be formulated into thin films, its poor mechanical and thermal properties limit the suitability for packaging applications. Since the properties of the packaging material directly affect the quality and the shelf life of

the product, suitable modifications are required. Several strategies have been tested and discussed in the literature to overcome the above-mentioned drawbacks. Recent reviews discussed the chemical modifications such as crosslinking of biopolymer chains by crosslinking agents via intra- or intermolecular linkages which enhanced the mechanical and barrier properties of the biopolymers. Moreover, the excess amount of the crosslinking agents can act as plasticizer agents [19]. Biopolymers such as starch, cellulose, alginate, pectin, glucose, and some proteins including gelatin have been blended with chitosan to improve the quality of food [16, 20].

Recent studies proposed various methods to enhance the properties by reinforcing numerous inorganic materials into the chitosan polymer matrix. Reinforcing nanomaterials such as nanohydroxyapatite [18, 21, 22], nano-MgO [6], nanoclays including montmorillonite [1, 23], and halloysite nanotubes [24, 25] had been incorporated, and numerous physicochemical properties of the packaging materials have been enhanced. Moreover, incorporation of graphene oxide and carbon nanotubes has successfully increased the mechanical properties of the films [3, 16]. Chitosan has been tested for antimicrobial studies due to its inherent antibacterial properties against both gram-positive and gram-negative bacteria and fungi. Reinforcement of Ag nanoparticles in a small percentage inactivated *E. coli* compared with the neat chitosan [26]. Ag nanoparticles have the ability to enter the microbial cells and induce the damage of the cell membrane and the reactions that damage the DNA of the cells [27]. Furthermore, incorporation of both zinc oxide (ZnO) nanoparticles and silver (Ag) nanoparticles into chitosan to form CH/Ag/ZnO blend had prevented the growth of microbial pathogens than CH/Ag and CH/ZnO films [26]. Stronger antibacterial properties against *S. aureus* than *E. coli* were exhibited by different kinds of graphene oxide- (GO-) chitosan nanohybrids (pristine powder, sphericle, and nanofibrilar network structures) [28]. Yadav et al. discussed a synthesizing route of cellulose/iron oxide nanocomposite [29] which enhanced the properties significantly. Chitosan-Fe-Al-Mn oxyhydroxide composites have been developed by Chaudhary et al. targeting adsorption applications [30]. To the best of our knowledge, there is no attempt that has been taken to incorporate iron oxide-based nanofillers into the chitosan structure targeting active packaging applications. But in conventional production, these nanomaterials are pricey, require a lot of time and effort, and most of all are not industrially viable. Nevertheless, the nanomaterials used in this study are extracted directly from an earth material called laterites. As stated in the method developed by the authors previously [31], these nanoparticles are cost-effective and industrially viable.

In this work, we reinforced CH polymer films by hematite nanoparticles (HNPs) and akaganeite nanoparticles (ANPs) by developing polymer nanocomposites and investigated their properties in relation to advanced green packaging applications. Hematite and akaganeite nanoparticles were synthesized using naturally occurring widely distributed ferruginous laterites [31, 32], and these nanoparticles were incorporated into CH by solution casting. The morphological, thermal, chemical, optical, and mechanical properties of synthesized nanocomposites were investigated using SEM, XRD, TGA, FTIR, UV-Vis-IR spectrometer, and tensile tester. The materials, chemicals, and methods used in this synthesis process are cost-effective, facile, and easily industrialized. Also, the iron oxide/hydroxide nanomaterials that were used to reinforce the chitosan matrix are nontoxic and environmentally friendly [33, 34]. Herein, eco-friendly polymer nanocomposites with enhanced properties are introduced, which could be considered as promising alternatives for petroleum-derived materials in future active packaging activities.

2. Experimental

2.1. Materials. Chitosan flakes from shrimp shells (molecular weight ~50000 Da based on viscosity; ≥75% of deacetylation), acetic acid (≥99.8%), sodium hydroxide (≥98.0%), hydrochloric acid (≥39 wt. %), and urea (99%) were purchased from Sigma-Aldrich and were used without further purification. Laterite rock samples were collected from Homagama, Sri Lanka.

2.2. Urea-Assisted Synthesis of ANPs and HNPs Using Ferruginous Laterite. Extraction of Fe^{3+} ions from laterites to the acid solution was performed by mixing 10 g of laterite powder (250 μm particle size), 20 ml of 5 M HCl solution, and 20 ml of distilled water under reflux condition for 5 h at 100°C as in [31]. The supernatant was separated by filtration and treated with 5 g of urea under reflux conditions at 90°C for 5 h. The resultant precipitate was separated by centrifugation, washed by 3 sediment-decant cycles, and oven-dried to get ANPs. One portion of the dry precipitate was calcined at 650°C for 2 h in a muffle furnace to produce HNPs.

2.3. Fabrication of Chitosan/HNP and Chitosan/ANP Composite Films. 1 g of chitosan flakes was dissolved in 100 ml of 1% (*w*/*v*) acetic acid solution by stirring at 500 rpm for 12 h. The chitosan solution was filtered by 180 μm sieve to remove undissolved particles. In order to prepare chitosan/HNP composites with 0.25% and 1% (w/w%) filler compositions, a predetermined amount of HNPs was added to the chitosan solution under the vigorous stirring at 1000 rpm. The homogeneous dispersions obtained after 24 h magnetic stirring followed by 10-minute sonication were poured into 8 cm size Petri dishes and vacuum dried for 3 days at 50°C to evaporate the solvent. Remaining acetic acid in the resultant nanocomposite films was neutralized by 5 ml of 1 M NaOH solution and rinsed with distilled water. Composite films were peeled off from the Petri dishes and placed in a desiccator for further testing. A similar procedure was followed to synthesize chitosan/ANP composites where the various amounts of ANPs were added to the chitosan solution instead of HNPs.

2.4. Characterization of HNPs and Composite Films

2.4.1. Morphological Analysis. Synthesized ANPs, HNPs, and the fracture surfaces of the composite films were examined by

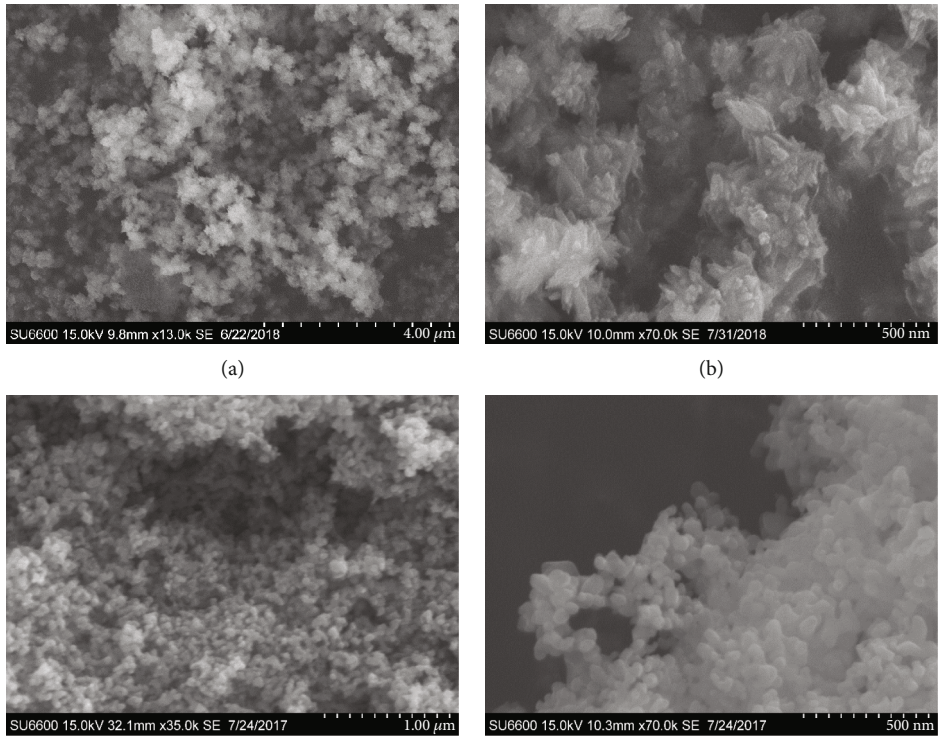

Figure 1: Scanning electron micrographs of nanofillers: (a, b) ANPs and (c, d) HNPs.

a field emission scanning electron microscope (FE-SEM) (Hitachi SU6600, Japan).

2.4.2. X-Ray Diffraction (XRD) Analysis. The crystallinity of the nanoparticles and the composite films were analyzed using diffraction patterns obtained from an X-ray diffractometer (Siemens D5000, Germany) working with an X-ray tube operated at 40 kV voltage and 40 mA current which emits Cu-Kα radiation. Data was collected at diffraction angle (2θ) values between 6° and 70° with step size of $2\theta = 0.1°$ at room temperature. The diffraction patterns were analyzed using the XPowder12 software package with the aid of the ICDD PDF-2 database.

2.4.3. Chemical Properties. Fourier-transform infrared (FTIR) spectra were analyzed using a spectrometer (Bruker VERTEX 80, USA) based on the Attenuated Total Reflection (ATR) technique within 500-4000 cm^{-1} with 32 scans per measurement and 4 cm^{-1} resolution to identify the interfacial interactions of the fabricated films.

2.4.4. Thermal Properties. Thermal behaviours of the composite samples between 25 and 800°C were determined using thermogravimetric analysis (TA Instruments SDT Q600, USA) with a ramp of 10°C/min in a nitrogen environment.

2.4.5. UV Shielding Properties. The UV absorbance of the produced films was examined over the range of 200-800 cm^{-1} using a UV-Vis-IR spectrophotometer (Shimadzu UV-3600, Japan).

2.4.6. Mechanical Properties. The average thicknesses of the test specimens were determined using a digital micrometer screw gauge (Mitutoyo, Japan) prior to the tensile tests. Thin film specimens with the dimensions of 8 mm × 70 mm were mounted on a cardboard window for ease of handling and fixed between the upper and lower clamps of the test rig with the gauge length of 35 mm. The maximum tensile strength (σ), elastic modulus (E), and elongation at break (ε) were performed as stated by ASTM D882-02 [35] using a tensile tester (Instron, USA) with a load cell of 500 kN and a strain rate of 5 mm/min. Six replicate thin film stripes were tested for each composition, and the mean values were reported.

2.4.7. Statistical Methods. One-way analysis of variance (ANOVA) was conducted by Tukey's post hoc test using commercially available software (IBM SPSS Statistics, version 21) to investigate the significant difference between the mean values of σ, E, and ε with respect to the HNP and ANP concentration. The mean difference was considered significant at the 0.05 level.

3. Results and Discussion

3.1. Morphologies of Nanomaterials. Laterite samples collected from the similar locality indicated that the composition consists of iron-bearing minerals, namely, goethite (FeO(OH)) and hematite (Fe_2O_3). The ferruginous nature of the laterite was a great advantage to use it as the iron source for the synthesis of nanoparticles. The iron extraction process from powdered laterite by hydrochloric acid solution

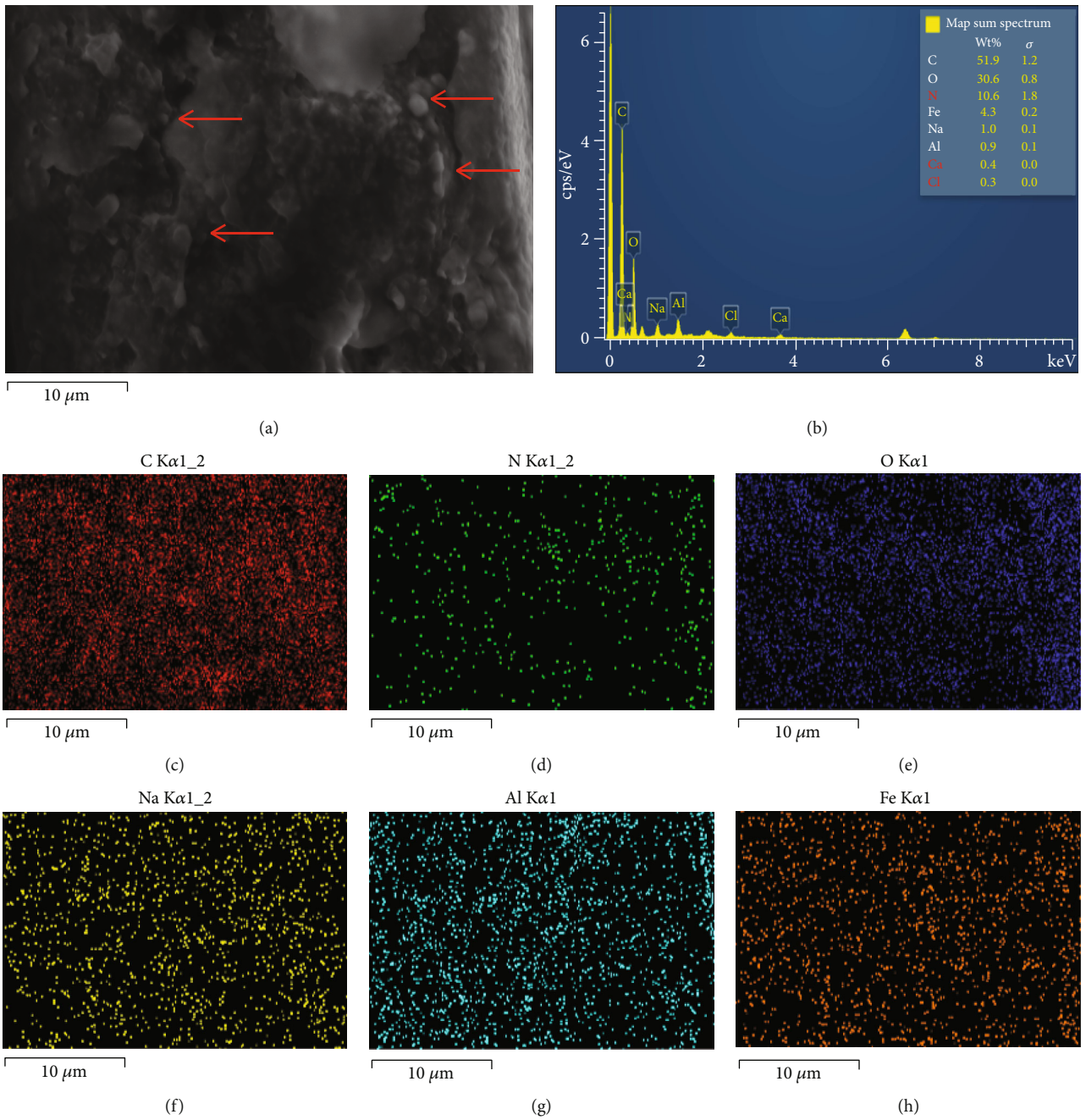

Figure 2: (a) Scanning electron micrograph, (b) EDS spectrum, and (c–h) elemental map layers of the selected site of the chitosan/0.25 (*w*/*w*%) ANP nanocomposite fracture surface.

and the urea-assisted nanoparticle synthesis method were discussed elsewhere [31]. Due to the low cost and noncomplexity, the above method was applied to produce hematite nanoparticles (HNPs) by calcination of akaganeite nanoparticles (ANPs).

The scanning electron micrographs of the HNPs and its precursor ANPs are presented in Figure 1. The precursor ANPs deemed to be a rice-like morphology where the HNPs exhibited nanoparticles in spherical to subhexagonal morphology. SEM images related to the fracture surfaces along with the EDS maps of the CH/HNP and CH/ANP composites are shown in Figures 2 and 3.

Nanoparticles embedded in the spaces of the CH matrix were clearly observed in SEM images and indicated by arrows. Multistep dispersion methods including mechanical stirring followed by ultrasound sonication have led to the homogenous dispersion of nanoparticles into the pore spaces of the polymer chains. The results were further confirmed by the elemental distribution pattern in the Fe layer of the EDS maps in both CH/HNP and CH/ANP composites.

3.2. X-Ray Diffraction Analysis. X-ray diffractograms of the polymeric compound, nanoparticles, and nanocomposites are shown in Figures 4 and 5. Two broad peaks at 11.9°-

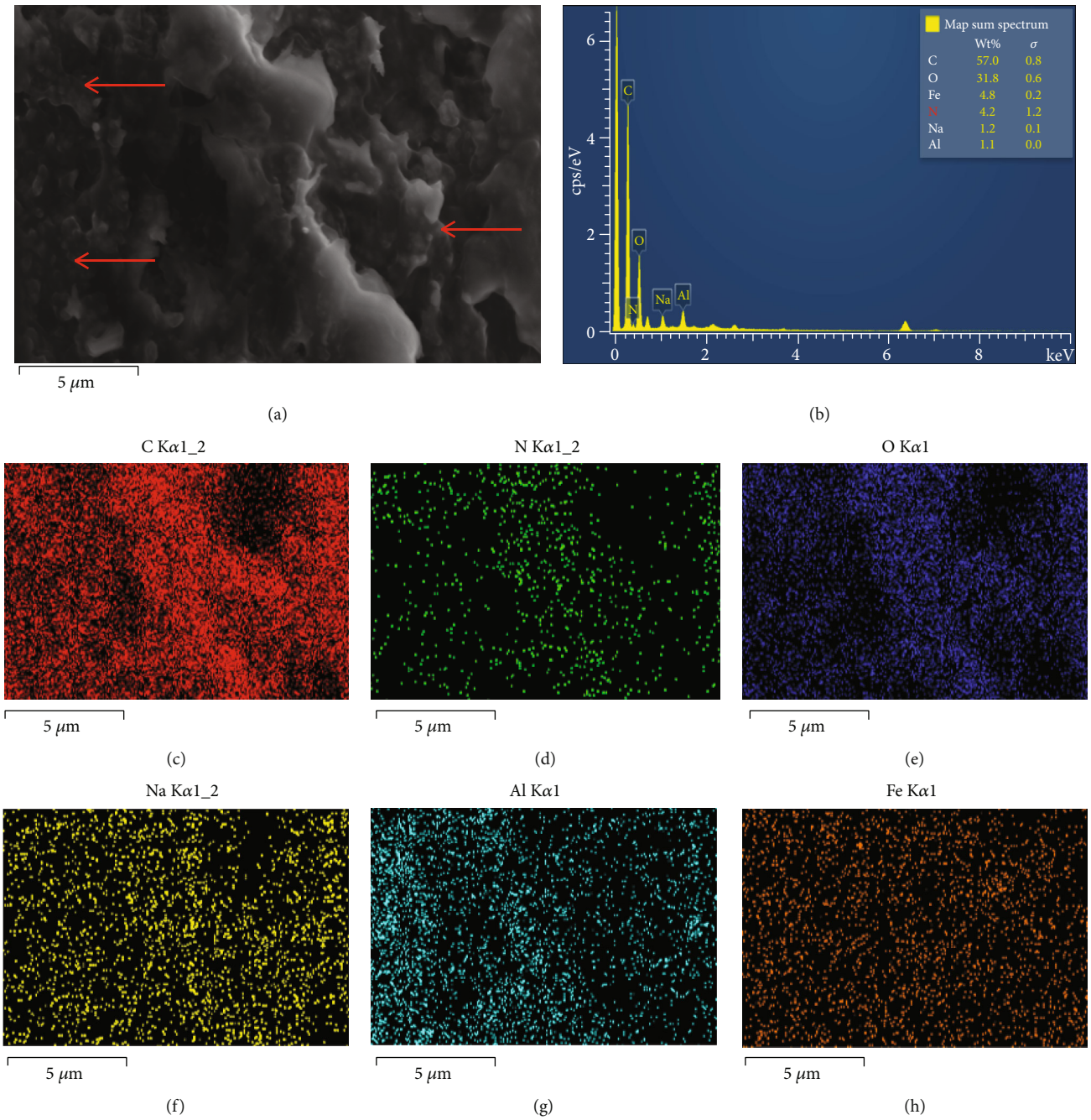

Figure 3: (a) Scanning electron micrograph, (b) EDX spectrum, and (c–h) elemental map layers of the fracture surface of chitosan/0.25 (*w*/*w*%) HNP nanocomposite.

17.5° and 20°-26° appeared in the diffractogram of chitosan (Figure 6) due to the amorphous nature of the polymeric compound. For HNPs (Figure 6), major diffraction peaks were found at 24.2°, 33.1°, 35.6°, 40.8°, 49.4°, and 54.0° related to (012), (104), (110), (113), (024), and (116) crystal planes, respectively. This crystallographic pattern is inherent in the hematite (Fe_2O_3) crystal structure (JCPDS card no. 0469-72). The resultant polymer nanocomposite (Figure 6) chitosan/HNPs exhibit two diffraction peaks at 33.1° and 35.6° related to hematite which confirms the reinforcement of HNPs into the CH.

Diffractogram related to ANPs exhibits peaks at 11.9°, 16.8°, 26.9°, 34.2°, 35.3°, 39.4°, 46.7°, 52.4°, and 56.2° related to 110, 200, 310, 400, 211, 301, 411, 600, and 521 crystal planes (Figure 7) and confirms the crystal structure of the akaganeite (FeO·OH) mineral (JCPDS card no. 0157-13).

3.3. Chemical Properties. The FTIR spectra of chitosan and chitosan/iron nanocomposites are shown in Figure 8. The dominant bands appearing in the neat chitosan are due to the vibrations of functional groups such as symmetrical stretching vibrations of N-H at 3356 cm^{-1}, stretching of

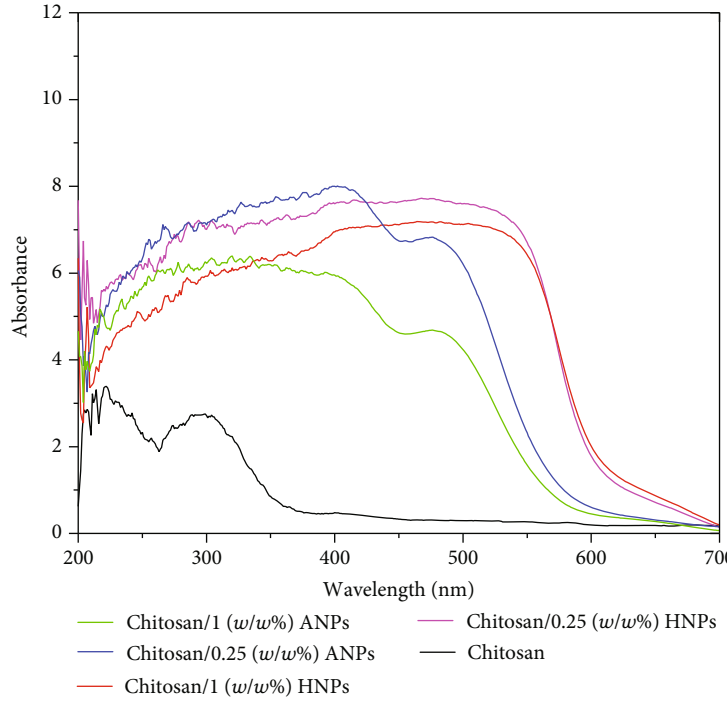

Figure 4: UV-Vis-IR spectra of the chitosan and nanocomposite films.

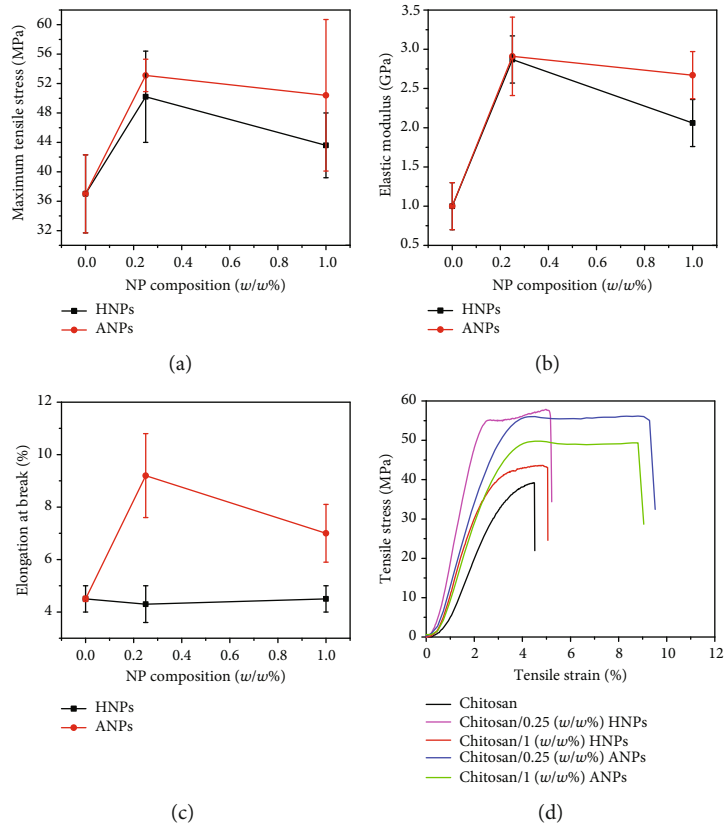

Figure 5: Plots of tensile properties, (a) maximum tensile stress, (b) elastic modulus, and (c) elongation at break, versus NP compositions and (d) stress-strain curves of polymer nanocomposites.

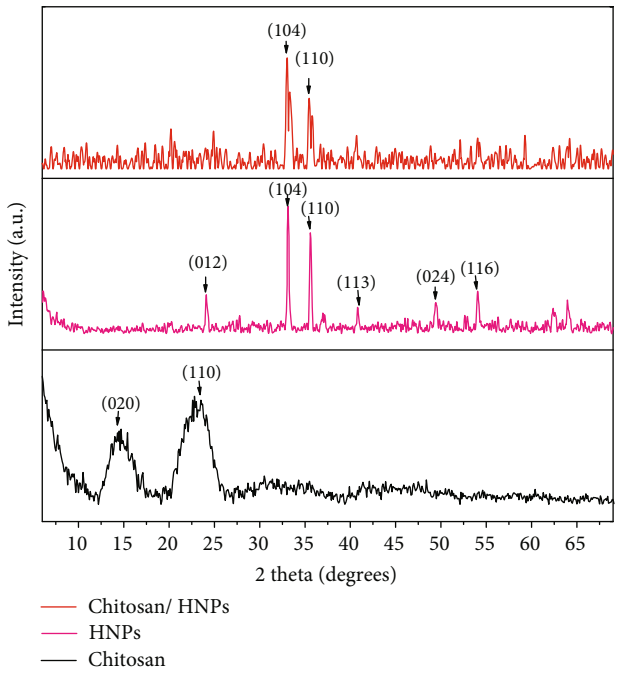

Figure 6: X-ray diffractograms of chitosan, HNPs, and chitosan/HNP nanocomposites.

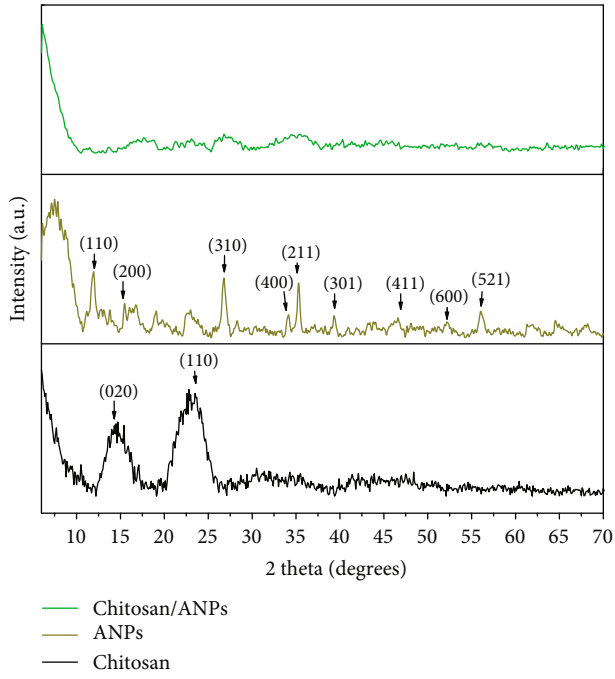

Figure 7: X-ray diffractograms of chitosan, ANPs, and chitosan/ANP nanocomposites.

-OH bonds corresponding to the strong and broadband centered at 3288 cm^{-1} [5], asymmetric stretching vibrations of C-H bonds at 2920 cm^{-1}, and stretching of C-H at 2874 cm^{-1}. Furthermore, vibrations of carbonyl bonds of the secondary amide group at 1647 cm^{-1}, C=O vibrations in the protonated amine group at 1566 cm^{-1}, CH bending of methylene at 1420 cm^{-1}, and a methyl group at 1377 cm^{-1} also indicate the characteristic peaks of chitosan. The peak at 1315 cm^{-1} is corresponding to the $-CH_3$ stretching vibrations of tertiary amide. The sharp peak centered at 1151 cm^{-1} is related to the asymmetric vibrations of CO. Moreover, the peak at 895 cm^{-1} indicates the wagging motions of the saccharide structure. The above vibrational patterns related to the bonds in the chitosan structure are frequently discussed in previous research works [36].

Each and every ATR-IR spectra of chitosan iron oxide nanocomposite comprises the above dominant peaks which denote the conserved chitosan structure after the production of nanocomposite films. As shown in Figure 8 inset 1, the peak corresponding to the C=O vibrations of the protonated amine group (1566 cm^{-1}) has been shifted towards the lower wavenumbers (1560 cm^{-1} with 0.25% HNPs, 0.25% ANPs, and 1% ANPs as well as 1558 cm^{-1} with 1% HNPs) by incorporating nanoparticles into the polymer. Additionally, the vibration band at 3288 cm^{-1} relevant to -OH bond stretching of chitosan indicates a wavenumber shift towards the lower direction. The value has been decreased as 3260 cm^{-1}, 3283 cm^{-1}, 3281 cm^{-1}, and 3275 cm^{-1} by reinforcing 0.25% HNPs, 1% HNPs, 0.25% ANPs, and 1% ANPs, respectively. This can be attributed to the possible interactions of iron nanoparticles along with the hydroxyl groups and amine groups of the chitosan skeleton through hydrogen bonding [6].

3.4. Thermal Properties. TGA curves for HNP- and ANP-reinforced chitosan composites are shown in Figure 9. A multistep decomposition pattern with 3 mass losses [6] was observed for all compositions. The mass loss near the 100°C region may be inherent in the removal of absorbed water and remaining solvents used during the casting step of the composite films. The rate of the mass loss increased when increasing the temperature from 250°C to 300°C which gave the next mass loss and decreased further when increasing the temperature giving third mass loss.

The second mass loss can be attributed to the degradation of amine and $-CH_2OH$ groups of the polymer. The third mass loss may be due to the decomposition of the glucosamine group of chitosan. 50% mass loss (WL) of chitosan was found at 325°C (Figure 9). At the same temperature conditions, the addition of 0.25 and 1 (w/w%) HNPs reduced the percentage mass loss into 26.74% and 16.89% while loading the same amount of ANPs decreased the mass loss into 48.42% and 38.03%, respectively. This improved thermal stability of nanocomposite films compared to that of neat chitosan is due to the impregnated hematite and akaganeite nanoparticles which have high heat resistivity. Furthermore, the particles act as a barrier to removal of the decomposed polymer matrix.

3.5. UV Shielding Properties. UV shielding ability is an important property of active packaging. Especially in light-sensitive foods, the photodegradation process can be undergone upon radiation during storage time. Figure 4 indicates the UV-Vis-IR absorbance spectra related to the neat CH and its nanocomposites. Absorbance measurements were conducted at different locations of the thin film samples,

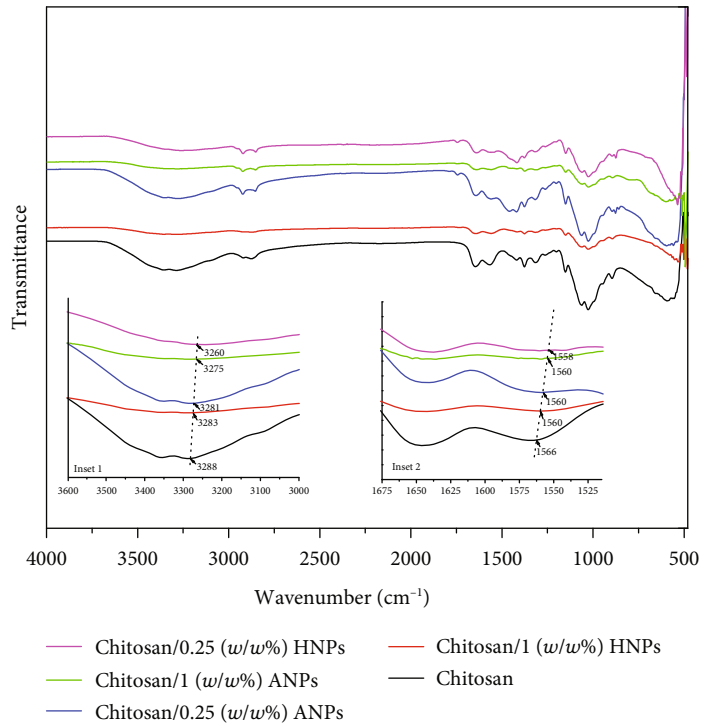

Figure 8: Fourier-transform infrared spectra of chitosan and nanocomposites.

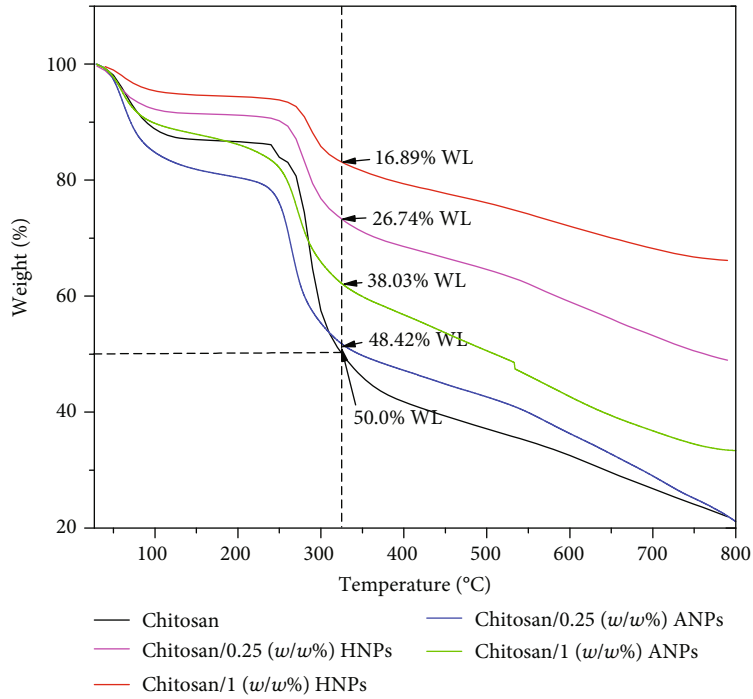

Figure 9: Thermogravimetric curves related to chitosan and nanocomposites.

and similar spectrum patterns were obtained. That could be due to the homogeneous dispersion of iron nanoparticles within the polymer. Nanocomposite samples were more effective than the pristine polymer in blockage of harmful UV radiation. The higher light absorption of wavelengths corresponding to the UV region by nanocomposites could be inherent in the reinforcement of HNPs and ANPs into the pores in the CH structure.

The UV shielding properties are higher in the lower wavelength UV (400 nm) and middle wavelength UV (500 nm). Compared to other chitosan composites, this material is a competent UV shielding material [6, 37, 38].

3.6. Mechanical Properties. Mechanical properties, namely, ultimate tensile stress (σ), elastic modulus (E), and elongation at break (ε), versus filler compositions and typical stress-strain curves of the nanocomposites are depicted in Figures 5(a)–5(d).

Statistical results obtained by one-way analysis of variance (ANOVA) along with Tukey's post hoc test indicated that there is a statistical significance ($P < 0.05$) between the mean values of σ among 0 and 0.25 (w/w%) HNPs, 0 and 0.25 (w/w%) ANPs, and 0 and 1 (w/w%) ANPs. Differences between the mean σ related to 0 and 1 (w/w%) HNPs and 0.25 and 1 (w/w%) HNPs as well as 0.25 and 1 (w/w%) ANPs are not significant. Optimum average σ values of the nanocomposites are deemed to be 50.2 ± 6.2 MPa and 43.6 ± 4.4 MPa with the addition of 0.25 (w/w%) HNPs and 1 (w/w%) HNP loadings, respectively, while 53.1 ± 2.3 MPa and 50.4 ± 10.3 MPa at 0.25 (w/w%) ANPs and 1 (w/w%) ANP loadings, respectively.

The differences between mean values of E are statistically significant in various compositions except for the difference between 0.25 and 1 (w/w%) ANP contents. E was improved by 187% and 106% by adding 0.25 (w/w%) and 1 (w/w%) HNPs while 191% and 167% by 0.25 (w/w%) and 1 (w/w%) ANP reinforcement to the polymer.

The ε value of the neat chitosan without nanofillers indicates 4.5 ± 0.5 GPa which was increased by 104% and 55.5% by adding 0.25 (w/w%) and 1 (w/w%) ANPs. In contrast, nanocomposites with 0.25 (w/w%) HNPs indicated 4.4% decrease of mean ε value with respect to the control sample. Differences between the mean ε of HNP compositions are not statistically significant. The difference between the ε values corresponding to each ANP composition is statistically significant ($P < 0.05$), other than the mean ε values between 0 (w/w%) and 1 (w/w%) ANPs. In that condition, the mean ε value was similar to the neat chitosan.

The addition of both nanofillers individually into the chitosan matrix has improved the tensile properties. The improvements in σ and E could be due to the interactions of hydroxyl and amine groups in chitosan with iron nanoparticles occurring via hydrogen bonding. This is further explained in Chemical Properties. Similar interactions had led to improvements in mechanical properties by incorporating different fillers such as nanoclay and MgO, which had facilitated the effective stress transfer from the matrix to the filler as a result of superior filler-matrix interaction [6, 24, 39]. Plots related to σ and E of both composite types followed similar patterns where there is an increasing trend from 0 to 0.25 (w/w%) and decreasing trend after that until 1 (w/w%). All parameters related to tensile properties indicated optimum values at 0.25 (w/w%) compositions in both HNP and ANP filler loadings. However, further loading of both nanofillers to the polymer has led to the decrement of the properties which indicate the saturation of reinforcing ability. When the filler loading is higher than the optimum level, the particles tend to agglomerate by creating high-stress concentrations. In consequence, the material gets ruptured easily through the weak planes under an external force.

These results indicate that the nanometer scale iron oxide nanoparticles can be used as an effective filler material in the production of chitosan nanocomposites. Furthermore, various properties of the polymer nanocomposite can be tuned by varying the nanofiller loading. Also, this material is in good agreement with the previously reported materials that the chitosan matrix is reinforced by various materials like MgO nanoparticles, carbon nanotubes, and cellulose [6, 40, 41].

4. Conclusions

Chitosan/iron nanocomposite films were successfully prepared by incorporating either hematite nanoparticles or akaganeite nanoparticles using the solution casting method. Nanoparticles were synthesized using a novel iron source; laterites and HNPs yielded to be spherical to subhexagonal morphology with 45 nm average size, while ANPs yielded to be rice-like morphology. XRD results confirm the crystalline phases of HNPs and ANPs as hematite and akaganeite, respectively. Tensile tests revealed the improvements of mechanical properties of the samples where maximum tensile stress of the chitosan/HNP composites was improved by 35.7% and 17.8% by incorporating 0.25 and 1 (w/w%), respectively, while chitosan/ANP composites indicated 43.5% and 36.2% enhancement with 0.25% and 1% (w/w%) reinforcement. Chemical properties evaluated by FTIR explained possible interfacial interactions of iron nanoparticles along with hydroxyl and amine groups in the chitosan skeleton. The TGA results indicate the enhancement of thermal properties due to thermal resistivity of the filler counterparts in composite films. Furthermore, the UV blocking ability of the nanocomposites was significant than unmodified chitosan films. The incorporation of a small amount of two nanofiller types into chitosan has led to the nanocomposite with enhanced physicochemical properties which can be considered as promising materials for packaging applications in the future.

Data Availability

The analytical data used to support the findings of this study are available from the corresponding author upon request.

Conflicts of Interest

The authors declare that they have no conflicts of interest.

Authors' Contributions

D.M.S.N. Dissanayake and G.T.D. Chandrakumara contributed to the manuscript equally and co-first authors.

Acknowledgments

This research was funded by the National Research Council of Sri Lanka, grant number 16-123. The authors would like to acknowledge all the staff members of the Sri Lanka Institute of Nanotechnology for the support and guide in instrumentation and analytical facilities.

References

[1] N. Bumbudsanpharoke and S. Ko, "Nanoclays in food and beverage packaging," *Journal of Nanomaterials*, vol. 2019, Article ID 8927167, 13 pages, 2019.

[2] A. Giannakas, C. Salmas, A. Leontiou, D. Tsimogiannis, A. Oreopoulou, and J. Braouhli, "Novel LDPE/chitosan rosemary and Melissa extract nanostructured active packaging films," *Nanomaterials*, vol. 9, no. 8, p. 1105, 2019.

[3] I. S. Fahim, N. Marei, H. G. Salem, and W. Mamdouh, "Effect of graphene and fullerene nanofillers on controlling the pore size and physicochemical properties of chitosan nanocomposite mesoporous membranes," *Journal of Nanomaterials*, vol. 2015, Article ID 979561, 10 pages, 2015.

[4] S. H. Othman, N. R. A. Kechik, R. A. Shapi'i, R. A. Talib, and I. S. M. A. Tawakkal, "Water sorption and mechanical properties of starch/chitosan nanoparticle films," *Journal of Nanomaterials*, vol. 2019, Article ID 3843949, 12 pages, 2019.

[5] E. A. Takara, J. Marchese, and N. A. Ochoa, "NaOH treatment of chitosan films: impact on macromolecular structure and film properties," *Carbohydrate Polymers*, vol. 132, pp. 25–30, 2015.

[6] R. T. De Silva, M. M. M. G. P. G. Mantilaka, S. P. Ratnayake, G. A. J. Amaratunga, and K. M. N. de Silva, "Nano-MgO reinforced chitosan nanocomposites for high performance packaging applications with improved mechanical, thermal and barrier properties," *Carbohydrate Polymers*, vol. 157, pp. 739–747, 2017.

[7] H. Ehrlich, D. Janussen, P. Simon et al., "Nanostructural Organization of Naturally Occurring Composites—Part II: Silica-Chitin-Based Biocomposites," *Journal of Nanomaterials*, vol. 2008, Article ID 670235, 8 pages, 2008.

[8] S. Y. Lee, H. E. Shim, J. E. Yang, Y. J. Choi, and J. Jeon, "Continuous flow removal of anionic dyes in water by chitosan-functionalized Iron oxide nanoparticles incorporated in a dextran gel column," *Nanomaterials*, vol. 9, no. 8, p. 1164, 2019.

[9] A. Mukheem, S. Shahabuddin, N. Akbar et al., "Boron nitride doped polyhydroxyalkanoate/chitosan nanocomposite for antibacterial and biological applications," *Nanomaterials*, vol. 9, no. 4, p. 645, 2019.

[10] I. O. Silva, R. Ladchumananandasivam, J. H. O. Nascimento et al., "Multifunctional chitosan/gold nanoparticles coatings for biomedical textiles," *Nanomaterials*, vol. 9, no. 8, p. 1064, 2019.

[11] R. Nisticò, A. Bianco Prevot, G. Magnacca, L. Canone, S. García-Ballesteros, and A. Arques, "Sustainable magnetic materials (from chitosan and municipal biowaste) for the removal of diclofenac from water," *Nanomaterials*, vol. 9, no. 8, p. 1091, 2019.

[12] Y. Zhang, Y. Shi, B. Yan et al., "Flocculant-assisted synthesis of graphene-like carbon nanosheets for oxygen reduction reaction and supercapacitor," *Nanomaterials*, vol. 9, no. 8, p. 1135, 2019.

[13] A. El Hadrami, L. R. Adam, I. El Hadrami, and F. Daayf, "Chitosan in plant protection," *Marine Drugs*, vol. 8, no. 4, pp. 968–987, 2010.

[14] M. Z. Elsabee and E. S. Abdou, "Chitosan based edible films and coatings: a review," *Materials Science and Engineering: C*, vol. 33, no. 4, pp. 1819–1841, 2013.

[15] S. Shankar and J. W. Rhim, "Polymer nanocomposites for food packaging applications," in *Functional and Physical Properties of Polymer Nanocomposites*, A. Dasari and J. Njuguna, Eds., Wiley, 2016.

[16] H. Wang, J. Qian, and F. Ding, "Emerging chitosan-based films for food packaging applications," *Journal of Agricultural and Food Chemistry*, vol. 66, no. 2, pp. 395–413, 2018.

[17] R. M. Jin, N. Sultana, S. Baba, S. Hamdan, and A. F. Ismail, "Porous PCL/chitosan and nHA/PCL/chitosan scaffolds for tissue engineering applications: fabrication and evaluation," *Journal of Nanomaterials*, vol. 2015, Article ID 357372, 8 pages, 2015.

[18] M. A. Nazeer, E. Yilgor, and I. Yilgor, "Intercalated chitosan/-hydroxyapatite nanocomposites : promising materials for bone tissue engineering applications," *Carbohydrate Polymers*, vol. 175, pp. 38–46, 2017.

[19] F. Garavand, M. Rouhi, S. H. Razavi, I. Cacciotti, and R. Mohammadi, "Improving the integrity of natural biopolymer films used in food packaging by crosslinking approach: A review," *International Journal of Biological Macromolecules*, vol. 104, Part A, pp. 687–707, 2017.

[20] S. M. Noorbakhsh-Soltani, M. M. Zerafat, and S. Sabbaghi, "A comparative study of gelatin and starch-based nanocomposite films modified by nano-cellulose and chitosan for food packaging applications," *Carbohydrate Polymers*, vol. 189, pp. 48–55, 2018.

[21] L. Pighinelli and M. Kucharska, "Chitosan-hydroxyapatite composites," *Carbohydrate Polymers*, vol. 93, no. 1, pp. 256–262, 2013.

[22] R. De Silva, P. Pasbakhsh, A. J. Qureshi, A. G. Gibson, and K. L. Goh, "Stress transfer and fracture in nanostructured particulate-reinforced chitosan biopolymer composites : influence of interfacial shear stress and particle slenderness," *Composite Interfaces*, vol. 21, no. 9, pp. 807–818, 2015.

[23] S. I. Hong, J. H. Lee, H. J. Bae et al., "Effect of shear rate on structural, mechanical, and barrier properties of chitosan/-montmorillonite nanocomposite film," *Journal of Applied Polymer Science*, vol. 119, no. 5, pp. 2742–2749, 2011.

[24] R. T. De Silva, P. Pasbakhsh, K. L. Goh, S. P. Chai, and H. Ismail, "Physico-chemical characterisation of chitosan/halloysite composite membranes," *Polymer Testing*, vol. 32, no. 2, pp. 265–271, 2013.

[25] B. Huang, M. Liu, and C. Zhou, "Chitosan composite hydrogels reinforced with natural clay nanotubes," *Carbohydrate Polymers*, vol. 175, pp. 689–698, 2017.

[26] M. Hosseinnejad and S. M. Jafari, "Evaluation of different factors affecting antimicrobial properties of chitosan," *International Journal of Biological Macromolecules*, vol. 85, pp. 467–475, 2016.

[27] M. Hoseinnejad, S. M. Jafari, and I. Katouzian, "inorganic and metal nanoparticles and their antimicrobial activity in food packaging applications," *Critical Reviews in Microbiology*, vol. 44, no. 2, pp. 161–181, 2017.

[28] H. J. Majidi, A. Babaei, Z. A. Bafrani, D. Shahrampour, E. Zabihi, and S. M. Jafari, "Investigating the best strategy to diminish the toxicity and enhance the antibacterial activity of graphene oxide by chitosan addition," *Carbohydrate Polymers*, vol. 225, p. 115220, 2019.

[29] M. Yadav, S. Mun, J. Hyun, and J. Kim, "Synthesis and characterization of iron oxide/cellulose nanocomposite film," *International Journal of Biological Macromolecules*, vol. 74, pp. 142–149, 2015.

[30] M. Chaudhary, S. Rawat, N. Jain, A. Bhatnagar, and A. Maiti, "Chitosan-Fe-Al-Mn metal oxyhydroxides composite as highly efficient fluoride scavenger for aqueous medium," *Carbohydrate Polymers*, vol. 216, pp. 140–148, 2019.

[31] D. M. S. N. Dissanayake, M. M. M. G. P. G. Mantilaka, T. C. Palihawadana et al., "Facile and low-cost synthesis of pure hematite (α-Fe2O3) nanoparticles from naturally occurring laterites and their superior adsorption capability towards acid-dyes," *RSC Advances*, vol. 9, no. 37, pp. 21249–21257, 2019.

[32] T. D. Pham, H. H. Nguyen, N. V. Nguyen et al., "Adsorptive removal of copper by using surfactant modified laterite soil," *Journal of Chemistry*, vol. 2017, Article ID 1986071, 10 pages, 2017.

[33] K. Rajendran, S. Sen, G. Suja, S. L. Senthil, and T. V. Kumar, "Evaluation of cytotoxicity of hematite nanoparticles in bacteria and human cell lines," *Colloids and Surfaces B: Biointerfaces*, vol. 157, pp. 101–109, 2017.

[34] M. I. Mohamed, M. K. A. Mohammad, H. R. Abdul Razak, K. Abdul Razak, and W. M. Md Saad, "Nanotoxic profiling of novel iron oxide nanoparticles functionalized with perchloric acid and SiPEG as a radiographic contrast medium," *BioMed Research International*, vol. 2015, Article ID 183525, 7 pages, 2015.

[35] ASTM 882-46T, *Standard Test Method for Tensile Properties of Thin Plastic Sheeting 1*, American National Standards Institute, 2002.

[36] R. N. Wijesena, N. Tissera, Y. Y. Kannangara, Y. Lin, G. A. J. Amaratunga, and K. M. N. De Silva, "A method for top down preparation of chitosan nanoparticles and nanofibers," *Carbohydrate Polymers*, vol. 117, pp. 731–738, 2015.

[37] L. Cano, E. Pollet, L. Avérous, and A. Tercjak, "Effect of TiO_2 nanoparticles on the properties of thermoplastic chitosan-based nano-biocomposites obtained by mechanical kneading," *Composites Part A: Applied Science and Manufacturing*, vol. 93, pp. 33–40, 2017.

[38] Y.-S. Huang, S.-H. Yu, Y.-R. Sheu, and K.-S. Huang, "Preparation and thermal and anti-UV properties of chitosan/mica copolymer," *Journal of Nanomaterials*, vol. 2010, Article ID 513798, 6 pages, 2010.

[39] I. Malagurski, S. Levic, A. Nesic, M. Mitric, V. Pavlovic, and S. Dimitrijevic-brankovic, "Mineralized agar-based nanocomposite films : potential food packaging materials with antimicrobial properties," *Carbohydrate Polymers*, vol. 175, pp. 55–62, 2017.

[40] A. Khan, R. A. Khan, S. Salmieri et al., "Mechanical and barrier properties of nanocrystalline cellulose reinforced chitosan based nanocomposite films," *Carbohydrate Polymers*, vol. 90, no. 4, pp. 1601–1608, 2012.

[41] S.-F. Wang, L. Shen, W. D. Zhang, and Y. J. Tong, "Preparation and mechanical properties of chitosan/carbon nanotubes composites," *Biomacromolecules*, vol. 6, no. 6, pp. 3067–3072, 2005.